

## COMMUNICATION

[View Article Online](#)  
[View Journal](#) | [View Issue](#)


Cite this: *Phys. Chem. Chem. Phys.*,  
2016, 18, 11951

Received 14th December 2015,  
Accepted 9th March 2016

DOI: 10.1039/c5cp07711g

[www.rsc.org/pccp](http://www.rsc.org/pccp)

Since the discovery of the plant pathogen tobacco mosaic virus as the first viral entity in the late 1800s, viruses traditionally have been mainly thought of as pathogens for disease-resistances. However, viruses have recently been exploited as nanoplatforms with applications in biomedicine and materials science. To this aim, a large majority of current methods and tools have been developed to improve the physical stability of viral particles, which may be critical to the extreme physical or chemical conditions that viruses may encounter during purification, fabrication processes, storage and use. However, considerably fewer studies are devoted to developing efficient methods to degrade or recycle such enhanced stability biomaterials. With this in mind, we carry out all-atom nonequilibrium molecular dynamics simulation, inspired by the recently developed mid-infrared free-electron laser pulse technology, to dissociate viruses. Adopting the poliovirus as a representative example, we find that the primary step in the dissociation process is due to the strong resonance between the amide I vibrational modes of the virus and the tuned laser frequencies. This process is determined by a balance between the formation and dissociation of the protein shell, reflecting the highly plasticity of the virus. Furthermore, our method should provide a feasible approach to simulate viruses, which is otherwise too expensive for conventional equilibrium all-atom simulations of such very large systems. Our work shows a proof of concept which may open a new, efficient way to cleave or to recycle virus-based materials, provide an extremely valuable tool for elucidating mechanical aspects of viruses, and may well play an important role in future fighting against virus-related diseases.

## Picosecond infrared laser-induced all-atom nonequilibrium molecular dynamics simulation of dissociation of viruses

Viet Hoang Man,<sup>a\*</sup> Nguyen-Thi Van-Oanh,<sup>b</sup> Philippe Derreumaux,<sup>c</sup> Mai Suan Li,<sup>de</sup> Christopher Roland,<sup>a</sup> Celeste Sagui<sup>a</sup> and Phuong H. Nguyen<sup>\*f</sup>

### Introduction

A virus is a nanoscale particle with essential functions like infecting a host cell of a biological organism, replicating, packaging its nucleic acid, and exiting the cell. In this process, a virus usually moves through a broad range of chemical environments, and exhibits remarkable plasticity in structure and dynamics. The high degree of conformational instability is necessary for viruses to facilitate the delivery of the viral genome inside the host cell through a structural rearrangement of the capsid, with or without capsid dissociation into sub-units.<sup>1</sup> On the other hand, viruses must also be rigid enough to resist extreme environments such as high temperatures, non-neutral pH, and other harsh conditions to protect their genomic materials.<sup>2</sup> Since the discovery of the plant pathogen tobacco mosaic virus as the first viral entity in the late 1800s,<sup>3</sup> viruses traditionally have been mainly thought of as pathogens for disease-resistances. However, the dual mechanical characteristics of viruses have been recently exploited for many applications from medicine to materials, expanding the virology field to a wide range of research studies far beyond biology. For example, in medicine, the conformational instability of viruses is desirable for the development of viruses for gene therapy and targeted drug delivery, where they should be capable of dynamic rearrangement or disassembly, to deliver their cargo into target cells. In contrast, the mechanical stability of viruses is required for many applications, for example, vaccines, contrast agents, diagnostic agents, and building blocks for some nanomaterials, where they may encounter extreme physical or chemical conditions during purification, fabrication processes, storage and use. Therefore, much effort has been focused on the improvement of the physical stability of virus-based materials, employing different approaches such as engineering of intersubunit electrostatic interactions<sup>4</sup> and intersubunit disulfide bonds,<sup>5</sup> and using chemical procedures.<sup>6,7</sup> For excellent reviews of the methods, readers are referred to recent publications.<sup>8,9</sup> However, fewer studies are currently carried out to address an obvious concern: how to efficiently dissociate such purposely enhanced stability materials

<sup>a</sup> Department of Physics, North Carolina State University, Raleigh, NC 27695-8202, USA. E-mail: vhman@ncsu.edu

<sup>b</sup> Laboratoire de Chimie Physique, Université Paris-Sud XI, F91405 Orsay Cedex, France

<sup>c</sup> Laboratoire de Biochimie Théorique, UPR 9080 CNRS, IBPC, Université Denis Diderot, Paris Sorbonne Cité 13 rue Pierre et Marie Curie, 75005, Paris, France

<sup>d</sup> Institute of Physics, Polish Academy of Sciences, Al. Lotników 32/46, 02-668 Warsaw, Poland

<sup>e</sup> Institute for Computational Science and Technology, SBI building, Quang Trung Software City, Tan Chanh Hiep Ward, District 12, Ho Chi Minh City, Vietnam

<sup>f</sup> Laboratoire de Biochimie Théorique, UPR 9080 CNRS, IBPC, Université Paris 7, 13 rue Pierre et Marie Curie, 75005, Paris, France. E-mail: nguyen@ibpc.fr

without much damage to the surrounding environment? This concern should be important if one wants to translate the virus-based nanofabrication technology into real-world applications where the degradation and recycling of materials might be necessary. Just one intuitive example, in the experiment using the viral capsid as a scaffold to mineralize positively charged iron oxide nanoparticles,<sup>10</sup> is how to remove the scaffold without much damage to the nanoparticles? Obviously, the use of acidic conditions or high temperatures is not promising because nanoparticles and the surrounding medium are easily affected. Of course, having efficient virus dissociation methods is also important for disease-resistance.

In general, viruses are assembled from repeating subunits to form highly symmetrical, homogeneous architectures and stabilized by a highly cooperative nature of the hydrogen bond (H-bond) network. Because H-bonds are involved with the backbone carbonyl C=O atoms, which primarily participate in the amide I vibrational modes, one can excite the amide I modes, leading to the destabilization of the H-bond network and subsequently dissociation of the whole viruses. Indeed, this idea has been employed to dissociate protein self-assembled nanostructures. In their pioneering studies, by tuning the frequency of a mid-infrared free-electron laser to the amide I bands, Kawasaki and coworkers were able to dissociate various amyloid fibrils – the extremely stable structures were stabilized by a stable H-bond network into soluble monomers.<sup>11–14</sup> To explain this experimental finding, very recently, we have carried out laser-induced nonequilibrium molecular dynamics (NEMD) simulations to study the dissociation of various amyloid fibrils<sup>15</sup> as well as peptide nanotubes.<sup>16</sup> We have shown that the dissociation mechanism is due to the strong resonance between the laser field and the amide I vibrational modes of the nanostructures. Inspired by these experimental and theoretical studies, here we wish to show, as a proof of concept, that viruses can also be degraded by a free electron laser whose frequency is tuned to the vibrational frequency of the amide I bands of the viruses.

## System and simulations

Adopting the poliovirus as a first representative system, we carry out large-scale all-atom NEMD simulations to understand the dissociation mechanisms. Poliovirus is classified as an enterovirus within the Picornaviridae, a family that contains many human and animal pathogens.<sup>18</sup> It is extremely stable at very high pressures,<sup>19</sup> and environmental solutions such as fresh water and sewage.<sup>20</sup> The viral genome, a single-stranded, (+)-strand RNA of approximately 7500 nucleotides in length, is enclosed in the protein shell. Here, we only focus on the empty poliovirus, *i.e.*, there is no RNA inside the virus shell. The virus contains 4 subunits, VP1–VP4, arranged with icosahedral symmetry, and each subunit contains 60 identical proteins. Each protein in VP1, VP2, VP3 and VP4 is composed of 302, 272, 238 and 68 residues, respectively [Fig. 1]. The initial structure was kindly provided by Okazaki and coworkers from the last structure of the 200 ns equilibrium molecular dynamics simulation trajectory,<sup>17</sup>

and is shown in Fig. 1(A) and (C). The structure is then solvated into an octahedral box containing 948 548 water molecules. This system is then neutralized by adding 1435 sodium ions, 1283 chloride ions, and 28 potassium ions, resulting in 3 659 530 atoms in total. We use the AMBER-f99SB-ILDN force field<sup>21</sup> to model the proteins and the TIP3P water model to describe the solvent. Starting from this structure, a short simulation of 1 ns is carried out in the *NPT* ensemble followed by another 1 ns *NVT* simulation, employing the GROMACS program.<sup>22</sup> Then 10 independent conformations are selected statistically from the *NVT* trajectory and subsequently used for the NEMD simulation.

In the NEMD simulation, a time-dependent electric field

$$E(t) = E_0 \exp\left[-\frac{(t-t_0)^2}{2\sigma^2}\right] \cos[2\pi c\omega(t-t_0)], \quad (1)$$

was applied to mimic a laser micro-pulse [Fig. 2(A)]. Here,  $E_0$  represents the amplitude of the electric field,  $\sigma$  is the pulse width,  $t$  is the time after the pulse maximum  $t_0$ ,  $c$  is the speed of light and  $\omega$  is the frequency. In a conventional molecular dynamics simulation, the temperature of the system is typically maintained by rescaling the velocities of all atoms at every time step.<sup>23</sup> In a laser-induced nonequilibrium experiment, the photoexcitation results in a vibrationally hot molecule, which is then cooled *via* the transfer of the vibrational energy to the surrounding solvent molecules.<sup>24</sup> Thus, in our NEMD simulations, only the waters are coupled to the heat bath in order to maintain the temperature of 310 K with a coupling constant of 0.1 ps. This technique has been developed in previous photo-induced NEMD simulations of peptides<sup>15,16,24–29</sup> and validated by comparing the cooling times with the known experimental results.<sup>24,27</sup> This also mimics the experimental conditions, in which water is added periodically to the suspension during the irradiation process in order to prevent excessive evaporating.<sup>11–14</sup> To ensure stability, a time step of 0.2 fs was used, and data were collected every 0.1 ps.

## Resonance between amide I vibrational modes and the laser field

The infrared free-electron laser developed by Kawasaki and coworkers to dissociate amyloid fibrils can generate a macro-pulse having a duration of 2 microsecond, each consisting of 2 ps micro-pulses separated by an interval of 350 ps. This means each macro-pulse contains about 6000 micro-pulses. The energy of a micro-pulse is in the range of 6–8 mJ. With this laser, fibrils are dissociated after several hours of radiation.<sup>11–14</sup> As we wish to use the infrared free-electron laser for dissociation of viruses, we set the pulse width  $\sigma = 2$  ps and  $t_0 = 8$  ps. Given the very large system-size and multiple trajectories are required, we varied the field strength and found that  $E_0 = 2$  V nm<sup>-1</sup> is sufficient so that the virus is dissociated within a reasonable timescale. As shown in the previous work,<sup>15</sup> the field strength does not affect the dissociation mechanism, but rather only accelerates or slowdowns the dissociation process. As our working assumption of the laser-induced dissociation method is the

resonance between the laser field and the amide I vibrational modes of the virus, we scan the laser frequency [eqn (1)] in the interval  $\omega = 1620\text{--}1720\text{ cm}^{-1}$  with a step of  $2\text{ cm}^{-1}$ , and carry out 500 NEMD simulations: 10 trajectories, each lasting 16 ps,

starting from the conformations selected from a 1 ns equilibrium MD trajectory at 310 K; each trajectory was run with 50 scanned values of  $\omega$ . To obtain the response of the virus to the field, we calculated the peak value of the C=O bond length fluctuation

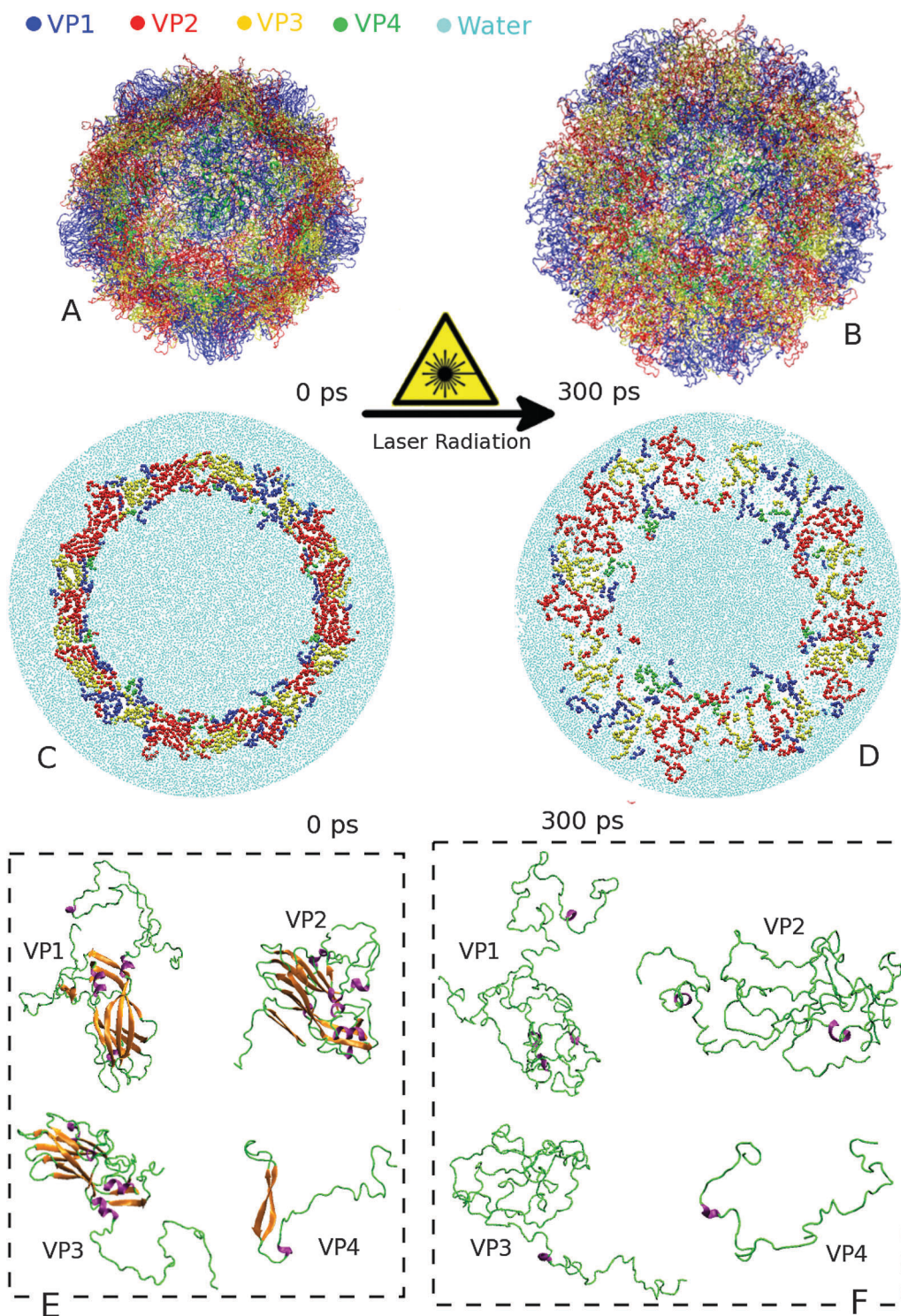


**Fig. 1** The equilibrium structure of the poliovirus obtained after the 200 ns equilibrium molecular dynamics trajectory provided by Okazaki and coworkers<sup>17</sup> (A and C) and after 300 ps laser-induced NEMD simulation (B and D). Above panels are the 3D structures and below are the cross-sections. The virus is composed of 4 repeating subunits V1–V4 formed by four different proteins which are shown in (E) before excitation and (F) after 300 ps of laser-induced dissociation. Water molecules are shown in cyan.

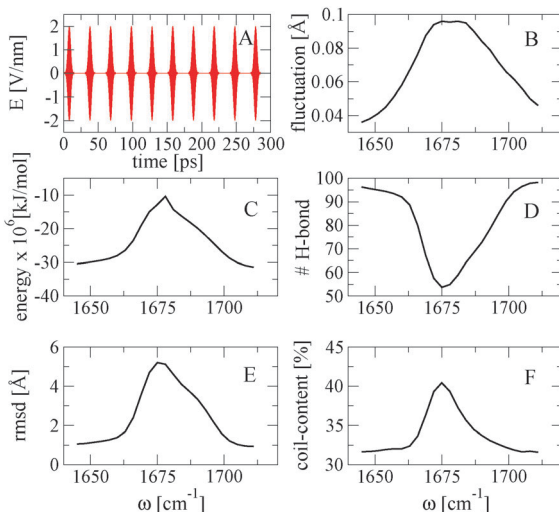


**Fig. 2** (A) Time evolution of the 10 electric field pulses with  $\omega = 1675 \text{ cm}^{-1}$ ,  $E_0 = 2 \text{ V nm}^{-1}$ , the laser-induced changes of the C=O amide bond lengths (B), the system energy (C), the intramolecular H-bonds (D), the RMSD (E) and the coil secondary structure content (F). The results are shown for the laser amplitude  $E_0 = 2 \text{ V nm}^{-1}$  and different frequencies  $\omega$ .

$$\langle \Delta d_{\text{CO}}(t) \rangle = (1/52560/10) \sum_{i=1}^{52560} \sum_{j=1}^{10} |d_i^j(t) - 1.23|, \text{ where } d_i^j(t) \text{ is the}$$

time evolution of the  $i$ -th C=O bond length (this virus consists of 52 560 C=O bonds) of the  $j$ -th trajectory and 1.23 Å is its equilibrium value. We also calculated the ensemble average of the last values (at 16-th ps) of the system energy, the intramolecular H-bond of individual chains, and the root-mean-squared deviation (RMSD) of the whole virus with respect to the initial structure, and secondary structures. As seen from Fig. 2, the virus exhibits a strong resonance with the field at  $\omega = 1675 \pm 2 \text{ cm}^{-1}$ , as indicated by large changes in the C=O bond lengths and the system energy [Fig. 2(B) and (C)]. This indicates that the laser excites primarily the amide I modes of the virus and that these are enough to dissociate the virus as clearly seen from a snapshot of the configuration shown in Fig. 1. More quantitatively, the dissociation is reflected by the decrease of the H-bond number from the equilibrium value of  $\approx 100$  to  $\approx 50$ , the RMSD increases from  $\approx 1 \text{ \AA}$  to  $\approx 6 \text{ \AA}$ , and proteins are converted to random coil structures [Fig. 2(D)–(F)].

## Laser-induced virus dissociation process

To investigate the dissociation process, starting from 10 selected equilibrium MD conformations, we carry out NEMD simulations, each lasting 300 ps. During this time, 10 micro-pulses with parameters ( $\sigma = 2 \text{ ps}$ ,  $t_0 = 8 \text{ ps}$ ,  $\omega = 1675 \text{ cm}^{-1}$ , and  $E_0 = 2 \text{ V nm}^{-1}$ ) separated by a time interval of 30 ps are applied to the system. We should note that the repetition rate of 30 ps is much shorter than the available experimental value of 350 ps, and difficult to generate in real experiments. Nevertheless, as our main aim is to provide a proof of concept, these laser parameters allow us to investigate the dissociation process within a reasonable timescale. As seen from Fig. 3, under the irradiation

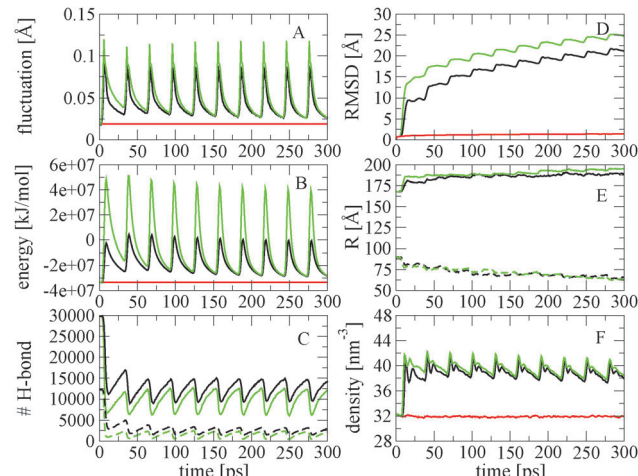


**Fig. 3** (A) Time evolution of the fluctuation of the C=O bond lengths; (B) the energy of the system; (C) the number of intra- (solid line) and inter-chain (dashed line) H-bonds; (D) the RMSD with respect to the initial structure; (E) the inner (dashed-line) and outer (solid-line) diameters of the virus; (F) the density of water molecules inside the virus. Shown are the results obtained from the NEMD simulation using 10 micro-pulses with  $\omega = 1675 \text{ cm}^{-1}$ ,  $E_0 = 2 \text{ V nm}^{-1}$  (black) and  $E_0 = 4 \text{ V nm}^{-1}$  (green). The results obtained from an equilibrium simulation are shown in red.

of the first pulse the resonance takes place and the amide I vibrational modes are excited after 5 ps, resulting in the large fluctuation of the C=O bond lengths with the maximal value of  $\approx 0.1 \text{ \AA}$  around 8 ps, which represents the peak of the laser pulse [Fig. 3(A)]. The excess C=O stretching potential energy is then converted to the kinetic energy, resulting in the increase of the total energy of the system which reaches the maximal value a bit later, around 9 ps [Fig. 3(B)]. After 8 ps, the laser intensity decreases and the fluctuations of the C=O bond lengths as well as the system energy are also reduced. As a consequence of the excitation, the intra- and intermolecular H-bonds formed in the equilibrium structures are excited, broken and quickly reduced from the initial values of  $\approx 3 \times 10^4$  and  $1.2 \times 10^4$  to  $\approx 1.1 \times 10^4$  and  $0.27 \times 10^4$ , respectively within the first 9 ps [Fig. 3(C)]. This leads to the destabilization of the virus as indicated by the increase of the RMSD with respect to the initial equilibrium structure from  $\approx 1$  to  $10 \text{ \AA}$  [Fig. 1(D)]. Interestingly, the virus is expanded in both inward and outward directions as indicated by the increase of the outer diameter from 168 to 180 Å, and the decrease of the inner diameter from 90 to 80 Å [Fig. 3(D)]. Although the virus wall is opened [Fig. 1(D)] but given the short excitation timescale of 10 ps, which is much shorter than the exchange rate of 25 μs between the waters inside and outside of the virus,<sup>17</sup> the waters largely remain inside the virus, therefore, the water density inside the virus increases from  $\approx 32$  to  $\approx 41 \text{ nm}^{-3}$  [Fig. 3(F)]. After 30 ps, the laser is turned on again and the second pulse excites the system one more time leading to further destabilization and this process is periodically repeated over 300 ps. Importantly, we observed an oscillation behavior of all quantities shown in Fig. 3, and to explain this, we calculated the Coulomb and van der Waals interactions and found that these two interactions are

comparable with  $\approx 55 \times 10^6 \text{ kJ mol}^{-1}$  for the Coulomb energy and  $\approx 7 \times 10^6 \text{ kJ mol}^{-1}$  for the van der Waals energy, indicating that both interactions play a role in the stabilization of the virus. This indicates that although the H-bond network is broken (Coulomb energy is reduced) during the increase of the laser intensity, after the pulse intensity decreases the van der Waals interaction forces the system to refold back closely to the structure at the end of the previous pulse, as indicated by the increase of the H-bonds as well as of the other structural quantities. This reflects the high degree of the plasticity of the virus, an important feature of most viruses which allows them to deliver their cargo into target cells. Understanding the factors that are responsible for the delicate balance between the virus reformation and dissociation might provide important insights into the functions of viruses and virus-based engineering. Although the structure after 300 ps reveals a large conformational rearrangement, the overall spherical shape is essentially maintained [Fig. 1]. This may imply that the virus delivers the viral genome inside the host cell through a structural rearrangement of the capsid without capsid dissociation into subunits.<sup>1</sup> For a comparison, we also carry out the simulation using a higher amplitude of the electric field,  $E_0 = 4 \text{ V nm}^{-1}$ , and as shown in Fig. 3, the dissociation process is quite similar to that obtained using  $E_0 = 2 \text{ V nm}^{-1}$ . This confirms further that the dissociation mechanism, which is induced by the resonance, depends much on the frequency rather than on the strength of the laser. Finally, we also carry out an equilibrium simulation ( $E_0 = 0 \text{ V nm}^{-1}$ ) and as seen from Fig. 3, the conformation of the virus is essentially unchanged.

The laser excitation results in the vibrationally hot virus, which is then cooled *via* the transfer of its vibrational energy to the surrounding water molecules, and it is great of interest to investigate the cooling process. To this end, we calculate the spatial distribution of the kinetic energy per atom crossing the simulation cell, and for the sake of clarity, Fig. 4 shows the cross-section of this distribution. At 0 ps, the system is in equilibrium at 310 K and every atom possesses a kinetic energy of  $3k_B T/2 \approx 3.9 \text{ kJ mol}^{-1}$ . The laser intensity reaches the maximal value at 8 ps, and results in the hot virus whose kinetic energy is  $\approx 22 \text{ kJ mol}^{-1}$ . However, as seen, the surrounding waters are still basically in the equilibrium state, indicating that the coupling to the heat bath is very efficient. In this context, our simulation technique that couples only waters to the heat bath mimics very well the experimental conditions, in which water is added periodically to the suspension during the irradiation process in order to prevent excessive evaporation.<sup>11–14</sup> After 30 ps, the first laser pulse is off, the virus is cooled down, and the kinetic energy reaches  $\approx 10 \text{ kJ mol}^{-1}$  at the center of the virus shell and  $\approx 6 \text{ kJ mol}^{-1}$  at the virus-water interface. After 10 pulses, the virus is largely dissociated, waters enter to the interior shell [Fig. 1(D)], thus the cooling is even more efficient as indicated by low ( $\approx 7 \text{ kJ mol}^{-1}$ ) and scattered kinetic energy distribution at 300 ps. Interestingly, due to the increase of the density [Fig. 3(F)], waters inside of the virus are more dense, resulting in the decrease of their mobility, and therefore, the kinetic energy of waters at the center of the virus is quite low ( $\leq 1 \text{ kJ mol}^{-1}$ ) at 300 ps.

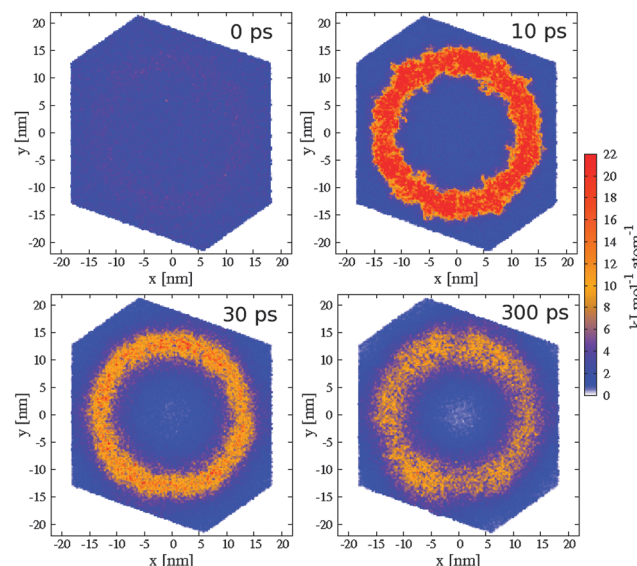


Fig. 4 The cross-section of the spatial distribution of the kinetic energy (in  $\text{kJ mol}^{-1}$ ) per atom in the simulation cell at selected times. Shown are the results obtained from the NEMD simulation using 10 micro-pulses with  $\omega = 1675 \text{ cm}^{-1}$  and  $E_0 = 2 \text{ V nm}^{-1}$ .

To investigate the dissociation process in more detail, we show in Fig. 5 the time-evolution of the secondary structures of proteins belonging to four subunits VP1, VP2, VP3 and VP4 (visualized in Fig. 1), calculated using the STRIDE program.<sup>30</sup> Interestingly, at the equilibrium, the secondary structures of VP1, VP2 and VP3 are quite similar with  $\approx 25\%$  for  $\beta$ ,  $\approx 35\%$  for turn,  $\approx 30\%$  for coil and  $9\%$  for the helix. For VP4, these structures are different with  $\approx 15\%$  for  $\beta$ ,  $\approx 33\%$  for turn,  $\approx 45\%$  for coil and  $9\%$  for the helix. Following the excitation, the  $\alpha$  and  $\beta$  structures pertained in four subunits are quickly destroyed and reduced to almost zeros. This is because the H-bond network which stabilizes these structures is broken due to the excitation of the C=O bonds. The turn and coil contents quickly increase to  $\approx 50\%$  and  $\approx 45\%$ , respectively, and then

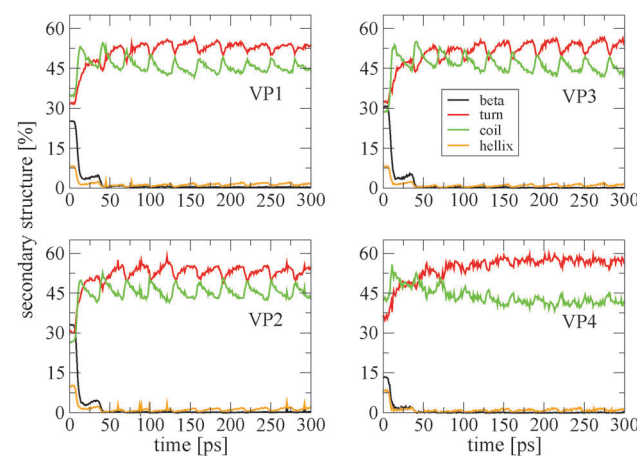
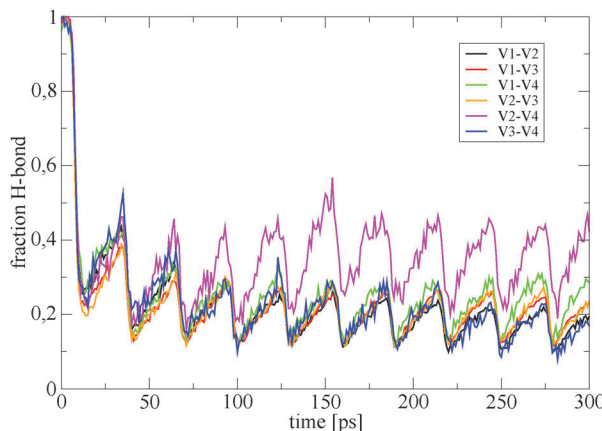


Fig. 5 Time evolution of various secondary structure contents of four subunits of the poliovirus virus following the laser excitation using 10 micro-pulses with  $\omega = 1675 \text{ cm}^{-1}$  and  $E_0 = 2 \text{ V nm}^{-1}$ .



**Fig. 6** Time evolution of the intermolecular H-bond between proteins pertained to two different subunits  $VP_i$  and  $VP_j$  ( $i, j = 1, 2, 3, 4$ ). Shown are the results obtained from the NEMD simulation using 10 micro-pulses with  $\omega = 1675 \text{ cm}^{-1}$  and  $E_0 = 2 \text{ V nm}^{-1}$ .

fluctuate around these values. These results indicate that the origin of the plasticity of the virus during its conformational rearrangement to deliver the genome maybe due to the interplay between the turn and coil structures of the VP1, VP2 and VP3 proteins. VP4 exhibits a lower degree of plasticity as indicated by the slow decay of the coil structure from  $\approx 45\%$  to  $40\%$  and the formation of the turn content of  $\approx 60\%$  at  $300 \text{ ps}$  [Fig. 5].

As mentioned above, the virus is highly spherical symmetric and to understand the relationship between structure-dissociation mechanisms, Fig. 6 shows the time-evolution of the total number of intermolecular H-bonds  $HB_{ij}$  between proteins of the  $VP_i$  and  $VP_j$  ( $i, j = 1, 2, 3, 4$ ). We note that because the number of residues of proteins pertained to subunits is different, the values of  $HB_{ij}$  are also different for different VP pairs. Thus, to facilitate a direct comparison, the results shown in Fig. 6 were normalized with respect to the equilibrium values at  $t = 0 \text{ ps}$ . Around  $9 \text{ ps}$  after the first laser pulse, all four subunits seem to break apart as indicated by  $\approx 80\%$  of reduction of  $HB_{ij}$  between every two subunits. After that, there is always a dissociation and reformation of the H-bond network between subunits as the virus responds to the field. Interestingly, the result shows a similar inter-subunit rearrangement behavior of subunits, except the  $HB_{24}$  exhibits a stronger tendency of the reformation of the VP2 and VP4 after 2 pulses ( $t \geq 60 \text{ ps}$ ). This indicates that, overall, the dissociation of the virus is almost isotropic, except a slightly strong resistance between VP2 and VP4. Understanding the factors that stabilize the interaction between VP2 and VP4 maybe important for the improvement of the physical stability of the viruses by protein engineering.

## Discussion and conclusion

We have presented comprehensive laser-induced NEMD simulations, and shown that by tuning the laser frequency precisely to that of the amide I vibrational mode, the resonance leads to the excitation of the virus to the high energy states, breaking off the weak links in the protein shell and dissociating the poliovirus. The implications of our new findings can be discussed as follows.

From the conception point of view, the use of the infrared laser to dissociate viruses may have two important implications, one is biological and one is technological. First, any new methods for killing viral particles may have important medical applications. Several photonic approaches have been developed such as UV and microwave treatments.<sup>31,32</sup> However, the UV irradiation targets both nuclei acids and proteins, so it damages not only the viral particles but also mammalian cells. The microwave absorption is not effective because most of the energy is transferred to water and not to the viral particles. Because of the difference in the nature of the H-bond network in viruses and nucleic acids, the infrared laser pulse targets the amide I bands of the viruses precisely, resulting in inactivating viruses without much harming the nucleic acids and surrounding. In this context, our theoretical study suggests that the infrared laser may well play an important role against virus-related diseases. On the technology front, viruses have recently been exploited as nanoplatforms with applications in biomedicine and materials science,<sup>33</sup> and their stability properties are even enhanced in purpose. Like any materials, they must, however, be recycled at some point during their lifetime and the degradation of such materials without much damage to the surrounding environment is challenging. The use of an infrared laser may open a new, efficient way to cleave or to recycle virus-based materials.

From the theoretical side, the large majority of all-atom molecular dynamics simulations were performed under equilibrium conditions to calculate thermodynamic mean values of small systems. So far the computational load has been so heavy that there are only a few all-atom simulations of very large systems such as entire viruses. In 2006, Schulten *et al.* performed 10 ns MD simulation of the satellite tobacco mosaic virus system consisting of over 1 million atoms to study the role of the RNA genome core in the stability of the virus.<sup>34</sup> Grubmueller *et al.* carried out force-probe simulation on the southern bean mosaic virus capsid with the system size of over 4.5 million atoms to compare with atomic force microscopy (AFM) studies.<sup>35</sup> May and Brooks performed 30 ns simulation of the Sesbania mosaic virus capsid of 800 000 atoms.<sup>36</sup> Van der Spoel *et al.* carried out 1  $\mu\text{s}$  simulation of the satellite tobacco necrosis virus with the system size of 1.2 million atoms to study the role of  $\text{Ca}^{+2}$  in stabilizing the capsid.<sup>37</sup> Finally, Okazaki and coworkers have generated a 200 ns trajectory of the poliovirus system consisting of over 6.5 million atoms,<sup>17</sup> using the highly parallelized MD program MODYLAS.<sup>38</sup> They examined the exchange rate of waters across the protein shell, and the pressure inside the capsid. Clearly, the low computer cost picosecond laser-induced NEMD simulations opens the door to study such and even larger systems so as to elucidate other structural and dynamical aspects of viruses.

Indeed, we first show that the virus is largely dissociated with the first excitation pulse ( $t \leq 15 \text{ ps}$ ), and the subsequent dissociation process is much slower because there is a balance between virus formation and dissociation, where the spherical shape is essentially maintained. This indicates that the initial partial and transient dissociated virus creates an energy barrier against further dissociation, acting like kinetic traps. In one of the disassembly experiments, Castellanos *et al.* have used AFM

experiments to mechanically induce dissociation of the minute virus of mice.<sup>39</sup> Their results reveal that the induced disassembly is frequently initiated by the loss of one capsomer leading to a stable, nearly complete particle that does not readily dissociate further. Zlotnick *et al.* have used a thermodynamic-kinetic model to show that during the early stages of dissociation of the hepatitis B virus (HBV), the nearly complete capsids were slow to dissociate further, but readily reassembled with free capsomers.<sup>40</sup> Our results are qualitatively consistent with these experimental and theoretical studies. These observations could imply that the virus may only undergo a structural rearrangement to deliver the viral genome rather than dissociating into subunits. Our all-atom simulations allow us to obtain further insights into the dynamical behavior at a molecular level and show that the plasticity of the virus is primarily due to the balance between the formation of the turn and coil structures of the constituent proteins. This finding may be important for protein engineering of viruses in medicine applications such as gene therapy and targeted drug delivery, where the conformational plasticity of viruses is desirable.

Also, Castellanos *et al.* have also shown that capsomers can be released from the capsid irrespective of where the force is applied on the viral particle.<sup>39</sup> Roos *et al.* have shown that the removal of some capsomers in very complex viral particles can be obtained either by AFM at different points or by a chemical treatment.<sup>41</sup> This is supported by our simulations showing that the virus is basically dissociated isotropically, even if there is a slight resistance between the subunits VP2 and VP4. These observations suggest that although force is directionally applied in AFM experiments, the same conformational dissociation may occur when energy is isotropically applied by chemical treatment or laser excitation. These could also support the coarse-grained simulation results of Brooks and coworkers which show that the cowpea chlorotic mottle virus only requires just one or two lowest frequency isotropic normal modes to account for the conformational changes.<sup>42</sup> Taken together, our laser-induced simulation approach has provided qualitatively theoretical support for those experimental and theoretical studies, and gained additionally some insights into the microscopic picture of the viruses and their dynamics at the molecular level.

## Acknowledgements

P. H. N is grateful to Dr Okazaki for kindly providing the initial structure of the virus. This work has been supported by CNRS, the National Science Foundation (NSF) USA *via* grant SI2-1148144 and 154941, the Department of Science and Technology, Ho Chi Minh City, Vietnam, and the IDRIS, CINES, TGCC centers for providing computer facilities (grant x2015077198).

## References

- 1 J. E. Johnson, Virus particle maturation: insights into elegantly programmed nanomachines, *Curr. Opin. Struct. Biol.*, 2010, **20**, 210–216.
- 2 C. Carrasco, M. Douas, R. Miranda, M. Castellanos, P. A. Serena, J. L. Carrascosa, M. G. Mateu, M. I. Marquas and P. J. de Pablo, The capillarity of nanometric water menisci confined inside closed-geometry viral cages, *Proc. Natl. Acad. Sci. U. S. A.*, 2009, **106**, 5475–5480.
- 3 M. W. Beijerinck, Concerning a contagium vivum fluidum as a cause of the spot-disease of tobacco leaves, *Verh. K. Akad. Wet. Amsterdam, Afd. Natuurkd.*, 1898, **6**, 3–21.
- 4 R. Mateo, E. Luna, V. Rincon and M. G. Mateu, Engineering Viable Foot-and-Mouth Disease Viruses with Increased Thermostability as a Step in the Development of Improved Vaccines, *J. Virol.*, 2008, **82**, 12232.
- 5 A. E. Ashcroft, H. Lago, J. M. Macedo, W. T. Horn, N. J. Stonehouse and P. G. Stockley, Engineering thermal stability in RNA phage capsids *via* disulphide bonds, *J. Nanosci. Nanotechnol.*, 2005, **5**, 2034.
- 6 H. R. Johnson, J. M. Hooker, M. B. Francis and D. S. Clark, Solubilization and stabilization of bacteriophage MS2 in organic solvents, *Biotechnol. Bioeng.*, 2007, **97**, 224.
- 7 M. J. Abedin, L. Liepold, P. Suci, M. Young and T. Douglas, Synthesis of a Cross-Linked Branched Polymer Network in the Interior of a Protein Cage, *J. Am. Chem. Soc.*, 2009, **131**, 4346.
- 8 M. G. Mateu, Virus engineering: functionalization and stabilization, *Protein Eng., Des. Sel.*, 2011, **24**, 53.
- 9 M. G. Mateu, Assembly, stability and dynamics of virus capsids, *Arch. Biochem. Biophys.*, 2012, **531**, 65.
- 10 T. Douglas, E. Strable, D. Willits, A. Aitouchen, M. Libera and M. Young, Protein Engineering of a Viral Cage for Constrained Nanomaterials Synthesis, *Adv. Mater.*, 2002, **14**, 415–418.
- 11 T. Kawasaki, J. Fujioka, T. Imai and K. Tsukiyama, Effect of Mid-infrared Free-Electron Laser Irradiation on Refolding of Amyloid-Like Fibrils of Lysozyme into Native Form, *Protein J.*, 2012, **31**, 710–716.
- 12 T. Kawasaki, J. Fujioka, T. Imai, K. Torigoe and K. Tsukiyama, Mid-infrared free-electron laser tuned to the amide I band for converting insoluble amyloid-like protein fibrils into the soluble monomeric form, *Lasers Med. Sci.*, 2014, **29**, 1701–1707.
- 13 T. Kawasaki, T. Imai and K. Tsukiyama, Use of a Mid-Infrared Free-Electron Laser (MIR-FEL) for Dissociation of the Amyloid Fibril Aggregates of a Peptide, *J. Anal. Sci., Methods Instrum.*, 2014, **4**, 9–18.
- 14 T. Kawasaki, T. Yaji, T. Imai, T. Ohta and K. Tsukiyama, Synchrotron-Infrared Microscopy Analysis of Amyloid Fibrils Irradiated by Mid-Infrared Free-Electron Laser, *Am. J. Anal. Chem.*, 2014, **5**, 384–394.
- 15 M. H. Viet, P. Derreumaux, M. S. Li, C. Roland, C. Sagui and P. H. Nguyen, Picosecond dissociation of amyloid fibrils with infrared laser: a nonequilibrium simulation study, *J. Chem. Phys.*, 2015, **143**, 155101.
- 16 M. H. Viet, P. M. Truong, P. Derreumaux, M. S. Li, C. Roland, C. Sagui and P. H. Nguyen, Picosecond melting of peptide nanotubes using an infrared laser: a nonequilibrium simulation study, *Phys. Chem. Chem. Phys.*, 2015, **17**, 27275.
- 17 Y. Andoh, N. Yoshii, A. Yamada, K. Fujimoto, H. Kojima, K. Mizutani, A. Nakagawa, A. Nomoto and S. Okazaki, All-atom molecular dynamics calculation study of entire poliovirus empty capsids in solution, *J. Chem. Phys.*, 2014, **141**, 165101.

- 18 V. R. Racaniello, One hundred years of poliovirus pathogenesis, *Virology*, 2006, **344**, 9–16.
- 19 D. Kingsley, D. G. Hoover, E. Papafragkou and G. P. Richards, Inactivation of hepatitis A virus and a calicivirus by high hydrostatic pressure, *J. Food Prot.*, 2002, **65**, 1605–1609.
- 20 R. L. Ward, D. R. Knowlton and P. E. Winston, Mechanism of inactivation of enteric viruses in fresh water, *Appl. Environ. Microbiol.*, 1986, **52**, 450–459.
- 21 K. Lindorff-Larsen, S. Piana, K. Palmo, P. Maragakis, J. L. Klepeis, R. O. Dror and D. Shaw, Improved side-chain torsion potentials for the Amber99SB protein force field, *Proteins: Struct., Funct., Bioinf.*, 2010, **78**, 1950–1958.
- 22 E. Lindahl, B. Hess and D. van der Spoel, GROMACS 3.0: A package for molecular simulation and trajectory analysis, *J. Mol. Model.*, 2001, **7**, 306–317.
- 23 H. J. C. Berendsen, J. P. M. Postma, W. F. van Gunsteren, A. Dinola and J. R. Haak, Molecular-dynamics with coupling to an external bath, *J. Chem. Phys.*, 1984, **81**, 3684–3690.
- 24 V. Botan, E. H. G. Backus, R. Pfister, A. Moretto, M. Crisma, C. Toniolo, P. H. Nguyen, G. Stock and P. Hamm, Energy transport in peptide helices, *Proc. Natl. Acad. Sci. U. S. A.*, 2007, **104**, 12749.
- 25 P. Nguyen and G. Stock, Nonequilibrium molecular dynamics simulation of a photoswitchable peptide, *Chem. Phys.*, 2006, **323**, 36.
- 26 P. Nguyen, R. D. Gorbunov and G. Stock, Photoinduced conformational dynamics of a photoswitchable peptide: A nonequilibrium molecular dynamics simulation study, *Biophys. J.*, 2006, **91**, 1224.
- 27 E. H. G. Backus, P. H. Nguyen, V. Botan, R. Pfister, A. Moretto, M. Crisma, C. Toniolo, G. Stock and P. Hamm, Energy transport in peptide helices: A comparison between high- and low-energy excitations, *J. Phys. Chem. B*, 2008, **112**, 9091.
- 28 S. Y. Park, P. H. Nguyen and G. Stock, Molecular dynamics simulation of cooling: Heat transfer from a photoexcited peptide to the solvent, *J. Chem. Phys.*, 2009, **131**, 184503.
- 29 P. H. Nguyen, S. Y. Park and G. Stock, Nonequilibrium molecular dynamics simulation of the energy transport through a peptide helix, *J. Chem. Phys.*, 2010, **132**, 025102.
- 30 D. Frishman and P. Argos, Knowledge-Based Protein Secondary Structure Assignment Proteins, *Proteins*, 1995, **23**, 566–579.
- 31 K. Rosenheck and P. Doty, The far ultraviolet absorption spectra of polypeptide and protein solutions and their dependence on conformation, *Proc. Natl. Acad. Sci. U. S. A.*, 1961, **47**, 1775.
- 32 J. C. Sutherland and K. P. Griffin, Absorption spectrum of DNA for wavelengths greater than 300 nm, *J. Radiat. Res.*, 1981, **86**, 399.
- 33 P. Singh, M. J. Gonzalez and M. Manchester, Viruses and their use in nanotechnology, *Drug Dev. Res.*, 2006, **67**, 23–41.
- 34 P. L. Freddolino, A. S. Arkhipov, S. B. Larson, A. McPherson and K. Schulten, Molecular dynamics simulations of the complete satellite tobacco mosaic virus, *Structure*, 2006, **14**, 437.
- 35 M. Zink and H. Grubmueller, Mechanical properties of the icosahedral shell of southern bean mosaic virus: a molecular dynamics study, *Biophys. J.*, 2009, **96**, 1350–1363.
- 36 E. R. May and C. L. Brooks, Determination of viral capsid elastic properties from equilibrium thermal fluctuations, *Phys. Rev. Lett.*, 2011, **106**, 188101.
- 37 D. S. D. Larsson, L. Liljas and D. van der Spoel, Virus Capsid Dissolution Studied by Microsecond Molecular Dynamics Simulations, *PLoS Comput. Biol.*, 2012, **8**, e1002502.
- 38 Y. Andoh, et al. MODYLAS: A Highly Parallelized General-Purpose Molecular Dynamics Simulation Program for Large-Scale Systems with Long-Range Forces Calculated by Fast Multipole Method (FMM) and Highly Scalable Fine-Grained New Parallel Processing Algorithms, *J. Chem. Theory Comput.*, 2013, **9**, 3201–3209.
- 39 M. Castellanos, R. Perez, P. J. P. Carrillo, P. J. D. Pablo and M. G. Mateu, Mechanical disassembly of single virus particles reveals kinetic intermediates predicted by theory, *Biophys. J.*, 2012, **102**, 2615–2624.
- 40 S. Singh and A. Zlotnick, Observed hysteresis of virus capsid disassembly is implicit in kinetic models of assembly, *J. Biol. Chem.*, 2003, **278**, 18249–18255.
- 41 W. H. Roos, K. Radtke, E. Kniesmeijer, H. Geertsema, B. Sodeik and G. J. Wuite, Scaffold expulsion and genome packaging trigger stabilization of herpes simplex virus capsids, *Proc. Natl. Acad. Sci. U. S. A.*, 2009, **106**, 9673–9678.
- 42 F. Tama and C. L. Brooks, Diversity and identity of mechanical properties of icosahedral viral capsids studied with elastic network normal mode analysis, *J. Mol. Biol.*, 2005, **345**, 299–314.